Theoretical-Experimental Correlation of Material Models for Nonlinear Deformation of Graphite

Robert M. Jones* and Dudley A.R. Nelson Jr.†
Southern Methodist University, Dallas, Texas

Two theoretical material models for nonlinear deformation of graphite due to Jones and Nelson are compared with Jortner's experimental results for uniaxial off-axis loading and biaxial loading of ATJ-S graphite specimens. The material models are extensions of the Jones weighted compliance matrix model and the Isabekian and Khachatryan restricted compliance matrix material model from linear to nonlinear deformation behavior. Both models include different behavior under tension loading than under compression loading.

Nomenclature

A_i, B_i, C_i, U_{0_i} = constants in ith material property equation [Eq. (19) of Ref. 1]
E_r, E_z, E_θ = Young's moduli in principal material directions
E_{rz}^{45} = Young's modulus at 45° to r and z directions
G_{rz} = shear modulus in rz plane
n = constant in energy weighting function [Eq. (22) of Ref. 1]
r, z, θ = radial, axial, and circumferential directions [Fig. 1 of Ref. 1]
x, y, z = rectangular coordinates in principal material directions
x', y', z' = rectangular coordinates in nonprincipal material directions
α = angle of orientation of off-axis tests
γ_{rz} = shear strain in rz plane
$\epsilon_r, \epsilon_z, \epsilon_\theta$ = strains in principal material directions
$\epsilon_{x'}, \epsilon_{y'}, \epsilon_{z'}$ = strains in x', y', z' directions
$\nu_{rz}, \nu_{r\theta}, \nu_{z\theta}$ = Poisson's ratios for principal material directions
$\sigma_r, \sigma_z, \sigma_\theta, \tau_{rz}$ = axisymmetric stresses in principal material coordinates

Subscripts

c = compression
t = tension

Introduction

TWO nonlinear multimodulus material models developed by Jones and Nelson[1] are correlated with experimental strain results for ATJ-S graphite to determine the accuracy of the models. The material models are extensions of the Jones weighted compliance matrix (WCM) model[2] and the Isabekian and Khachatryan restricted compliance matrix (RCM) model[3] for different behavior under tension loading than under compression loading. The extensions consist of accounting for the various nonlinear stress-strain curves in the manner of Jones and Nelson.[4,5] They relate the secant modulus properties of the stress-strain curves to the strain energy of an equivalent elastic system. Thus, interaction between all stress components is assured in this new deformation theory of orthotropic plasticity.

The paper is divided in two major parts: 1) uniaxial strain correlations for off-axis loading and 2) biaxial strain correlations. In each part, the strains predicted with both material models are compared with measured strains. The experimental results are due to Jortner[6-10] and consist of strains from uniaxial loading of bar and rod specimens in nonprincipal material directions (off-axis loading) and from biaxial loading of tubular specimens.

Comparison of Predicted and Measured Strains Under Uniaxial Off-Axis Loading

The two nonlinear multimodulus material models are used to predict the uniaxial deformation behavior of ATJ-S graphite when load is applied at angle α to the principal material directions. These predictions are compared with the strain response measured by Jortner[9] to evaluate how well the

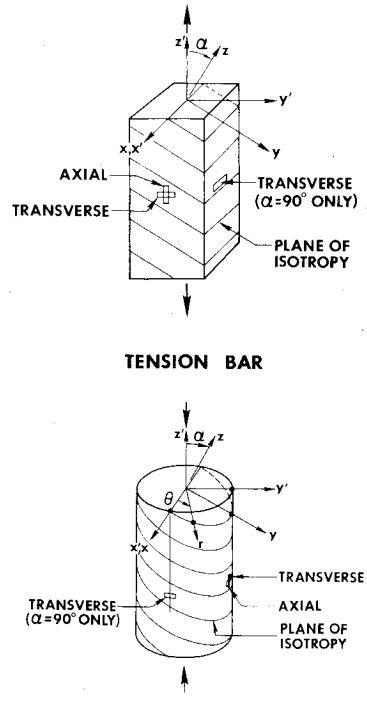

Fig. 1 Tension bar and compression rod gage sections.

Presented as part of Paper 75-769 at the AIAA/ASME/SAE 16th Structures, Structural Dynamics, and Materials Conference, Denver, Col., 27-29 May 1975. Received Nov. 14, 1975: revision received Feb. 23, 1976. This research was sponsored by Air Force Materials Laboratory Contract F33615-73-C-5124 and Air Force Office of Scientific Research/NA Grant 73-2532.

Index categories: Materials, Properties of; Structural Composite Materials (including Coatings); Structural Static Analysis.

*Professor of Solid Mechanics. Associate Fellow AIAA.

†Research Assistant. Now Senior Engineer, McDonnell-Douglas Technical Services Co., Houston, Tex. 77058. Member AIAA.

uniaxial deformation behavior can be predicted when load is applied in: 1) principal material directions and 2) other than principal material directions.

Description of Test Specimens and Procedures

Jortner's off-axis specimens[9] are obtained from ATJ-S graphite billet 16K9-27. The billet cylindrical coordinate system is nominally aligned with the principal material directions. That is, the principal material directions are not necessarily the same throughout the billet because of nonuniformities in the billet manufacturing process, e.g., nonuniform compaction or nonuniform particle-binder mixture. Tension test specimens 6-in. long with a ¼-in. square gage section and 2-in. long compression test specimens, which have the characteristic dogbone shape along with a ½-in. diameter cylindrical gage section, are shown in Fig. 1.

The $(x'\text{-}y'\text{-}z')$ coordinate systen used in the presentation of strain results is shown in Fig. 1. Note that the x-y-z coordinate system is aligned with the nominal principal material directions of the material and that the x and y coordinates are in the plane of isotropy of the material. The angle α is the angle in the y-z plane between the load axis (z') and the across-grain (z) principal material direction. For example, the specimen is loaded uniaxially in the across-grain (z) direction when $\alpha = 0°$ and in the with-grain (y) direction when $\alpha = 90°$. Strains are measured in the x'-y'-z' coordinate directions.

Acoustic velocity measurements and shear coupling effects on the specimens are reported by Jortner.[8] Acoustic velocities are measured to determine variations between local and nominal principal material directions due to billet nonuniformities. Jortner speculates that, for the 45° tension specimens and the 70° compression specimens, the angles between principal material and load directions may be close to 40° and 80°, respectively. For both the tension and compression specimens, the effect of shear coupling on the stress distribution across the width of the gage sections is small.

The specimens are loaded in an Instron machine. The load is introduced in the tension specimens through pin attachments to doublers bonded to the specimens. The compression specimens are loaded in a test fixture with an estimated friction-induced error in the recorded load of less than 2%.[9]

Material Properties

The first step in application of the new material models in strain correlation studies is to develop a set of material property constants for the material property - strain energy equations from appropriate uniaxial test results. The material property constants used in the present strain correlations are determined directly from Jortner's experimental results.[9] Thus, extraneous variations between predicted and measured strains are not introduced because of billet-to-billet variations in material properties or differences in test procedures. The material property constants in the billet coordinate system (principal material coordinates) are given in Table 1.

Table 1 Constants in material property equations for 16K9 billet data base[a] at 70°F

Material property	A	B	C	U_0
E_{rt}	1.72×10^6psi	0.102	0.446	1 psi
E_{zt}	1.37×10^6psi	0.232	0.255	1 psi
$\nu_{r\theta t}$	0.1	0.376	0.170	1 psi
$\nu_{z\theta t}$	0.16	0.446	0.158	1 psi
E^{45}_{rzt}	1.39×10^6 psi	0.133	0.365	1 psi
E_{rc}	1.52×10^6psi	0.061	0.647	1 psi
E_{zc}	1.15×10^6psi	0.140	0.370	1 psi
$\nu_{r\theta c}$	0.09	0	1	1 psi
$\nu_{z\theta c}$	0.1	0	1	1 psi
E^{45}_{rzc}	1.26×10^6psi	0.123	0.395	1 psi

[a]Experimental data due to Jortner,[9] Figs. 4, 5, 7, 9, 10, and 12.

Different independent material properties are required for each of the two nonlinear multimodulus material models. For a transversely isotropic multimodulus material, six independent material properties are needed to apply the restricted compliance matrix material model. The predictions with the RCM model depend on which material properties are selected for the uniaxial baseline values. Of course, any set of six material properties could be used, and the same predictions would result if the restrictions of the material model were perfectly satisfied by the stress-strain behavior of the material. For transversely isotropic multimodulus materials, ten independent material properties are required to apply the weighted compliance matrix material model.

The strains predicted with the nonlinear material model are shown by Jones and Nelson[5,11] to be within 5% of measured normal strains and somewhat less accurate for measured transverse strains under uniaxial off-axis tension loading. Moreover, the restricted compliance matrix model is identical to the weighted compliance matrix model under uniaxial stress conditions if the RCM model properties are measured with the same stress sign as the uniaxial stress. That is, we determine (arbitrarily) most of the RCM model properties in tension so all models, including the ordinary nonlinear material model,[4] are identical under uniaxial tension (all energy function differences vanish under these conditions). Thus, we need only investigate the restricted compliance matrix model for uniaxial compression. The input material property sets for the RCM model are

Property Set E_{zc}: E_{rt}, E_{zt}, $\nu_{r\theta t}$, $\nu_{z\theta t}$, E^{45}_{rzt}, E_{zc}

Property Set E_{rc}: E_{rt}, E_{zt}, $\nu_{r\theta t}$, $\nu_{z\theta t}$, E^{45}_{rzt}, E_{rc}

Method of Presentation of Results

Strain predictions with the new material models are shown in Figs. 2–5 as symbols next to the curves for experimental results. The experimental results are obtained from Jortner's Figs. 9–12 of Ref. 9. The predicted strains are obtained with

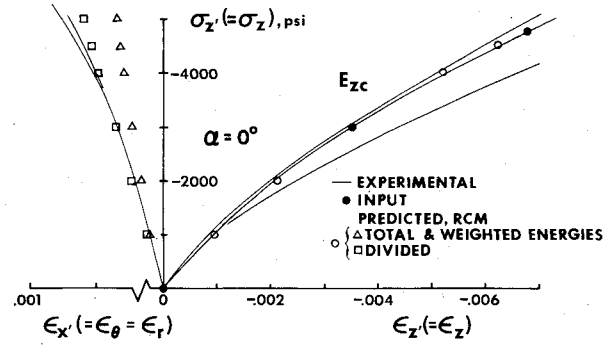

Fig. 2 Off-axis behavior—compression, $\alpha = 0°$, RCM, E_{zc}.

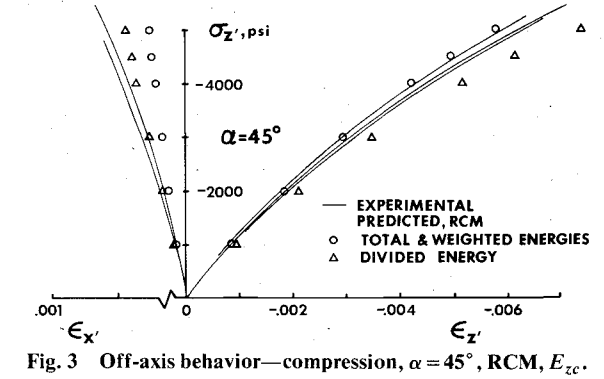

Fig. 3 Off-axis behavior—compression, $\alpha = 45°$, RCM, E_{zc}.

the MULTIR and MULTIW computer programs.[1] Different categories of strain predictions must be discussed because some of the experimental results are used to develop the material property constants input to these computer programs. The material property constants are determined by simultaneous solution from data at three points on the experimental curves. Predictions of strains for these data base points are shown as filled-in circles, whereas other predictions with the material model are shown as open circles. All the predictions along stress-strain curves used to define material property - strain energy relationships are distinguished from other predictions by the appearance of the material property designation next to its defining curve. For example, the experimental results in Fig. 2 are used to define the constants in the equation relating material property E_{zc} to the strain energy.

In the discussion of results, approximate percentage differences between predicted and measured strains are computed from

$$\Delta\epsilon = \frac{^{\epsilon}\text{Predicted} - {}^{\epsilon}\text{Measured}}{^{\epsilon}\text{Measured}} \times 100\% \qquad (1)$$

When more than one experimental curve exists for stress-strain behavior, the percentage differences are calculated between the predicted value and the average experimental results.

Compressive Strain Correlations for Nonlinear Restricted Compliance Matrix Model

The restricted compliance material model is applied for compressively loaded specimens to obtain the predicted results in Figs. 2-5. Results for material property sets E_{zc} and E_{rc} are displayed in Figs. 2-5 and in Ref. 11, respectively. Recall that the two material property sets differ by only one independent material property. The material property E_{zc} used in the first property set is replaced by E_{rc} in the second property set. All three energy approaches are investigated for material property set E_{zc}. Only the total energy approach is examined for the second property set E_{rc}. The dependence of the predictions with the RCM model on the selection of the baseline material properties is demonstrated with the results. The differences in transverse strain predictions for the total energy approach with the two different property sets are small (less than 5%) because the off-diagonal compliances are determined from the same independent material properties (tension properties) in both cases. Differences in transverse strain predictions occur because the material properties are determined at different total energy levels. The corresponding axial strain predictions with the different data sets are not the same. Thus, the relations between tension and compression compliances in the RCM model may not be applicable to ATJ-S graphite.

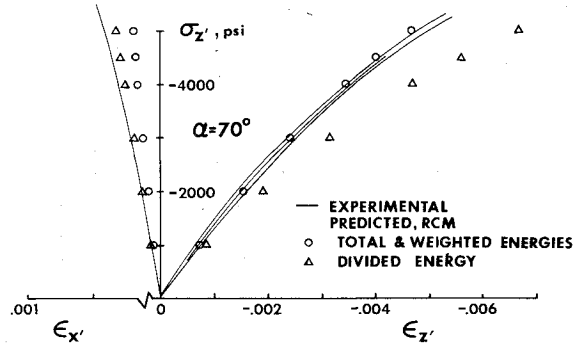

Fig. 4 Off-axis behavior—compression, $\alpha = 70°$, RCM, E_{zc}.

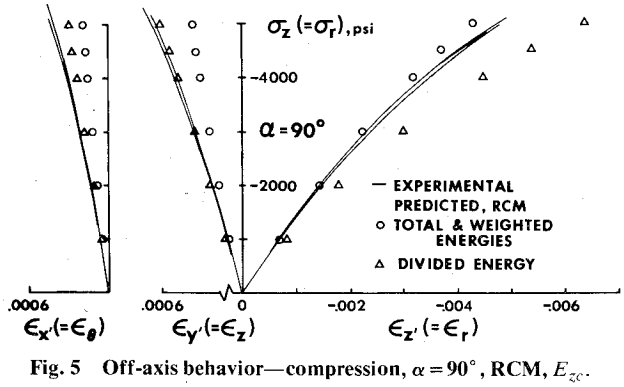

Fig. 5 Off-axis behavior—compression, $\alpha = 90°$, RCM, E_{zc}.

The predicted axial strains in Figs. 2-5 agree relatively well (within 10%) with test results for the total and weighted energy approaches. However, the transverse strain correlation is generally poor. The largest deviation in axial strains, −10%, occurs for the $\alpha = 90°$ case (Fig. 5). At −5000 psi, all transverse strain predictions for the total and weighted energy approaches in Figs. 2-5 differ from measured results by 45% to 57%. The relationships between diagonal compliances (direct moduli) for the all-tension and all-compression stress states in the nonlinear RCM model might be applicable to ATJ-S graphite, but those between off-diagonal compliances (in which both direct moduli and Poisson's ratios appear) are not applicable. The restrictions on the off-diagonal compliances in the nonlinear RCM model may be especially stringent for nonlinear stress-strain behavior of the material. When all material properties are evaluated at the same energy level, the compliance relationships should be valid. In the 70° F experimental results in Refs. 9 and 12, the tension Poisson's ratios generally decrease with increasing energy level, whereas Poisson's ratios in compression usually remain almost constant or increase. Thus, the variations for Poisson's ratios implied in the nonlinear RCM model may not be representative of the actual variations. When the divided energy approach is used in the nonlinear RCM model instead of the total or weighted energy approaches, the transverse strain correlation is somewhat improved (the largest deviation is about 29%), but the axial strain correlation is much poorer (the largest deviation is approximately 37%). With the divided energy approach, the implied off-diagonal compliances are constant on successive iterations for the loading and independent material properties investigated. The improved correlation for the transverse strain stems from the larger strain predictions in the divided energy approach than in the total or weighted energy approaches. These predictions occur because the implied off-diagonal compliances remain constant instead of decreasing with increasing energy level. The implied diagonal compliances in the divided energy approach are inappropriate as evidenced by the poor axial strain correlations.

Summary

The strain predictions with both the nonlinear restricted compliance and weighted compliance matrix material models are compared with the experimental strain response obtained from uniaxial loading of specimens with principal material directions at four different orientations with respect to the load axis. The best overall correlation between predicted and measured strains occurs for the nonlinear weighted compliance matrix material model. Note that the nonlinear weighted compliance matrix material model results are the same for all energy approaches under these uniaxial stress conditions. That is, because the stresses are either all tension or all compression, the three energies used in each of the three energy approaches are identical. Moreover, the compliances are all determined at the same energy level. In contrast, for the nonlinear restricted compliance matrix model, the total and weighted energies are the same, but the divided energy approach leads to the following undesirable consequence. Specifically, in an all-compression stress state, the com-

pression energy is the total energy and the tension energy is zero; accordingly, the compliances are determined from a mixed set of nonlinear compression properties and linear (elastic) tension properties. Thus, differences between measured strains and strains predicted with the nonlinear restricted compliance matrix material model are attributed mainly to the relations between tension and compression compliances used in the model. The stress-strain behavior of ATJ-S graphite does not closely satisfy the restrictions between compliances in the nonlinear RCM model.

The correlation is excellent between predicted and measured strains. Thus, the general material property equation, Eq. (19) of Ref. 1, can be used to represent the material property - strain energy variation for both tension and compression properties of ATJ-S graphite at 70°F.

Comparison of Predicted and Measured Strains Under Biaxial Loading

The two nonlinear multimodulus material models are used to predict the biaxial strain response of ATJ-S graphite. Strain predictions with both material models are compared with strains measured by Jortner[6-10] in room temperature tests. Strain predictions with the Jones-Nelson nonlinear material model are also compared with the biaxial tension strain response measured at room temperature. Thus, in the latter case, the basic nonlinear approach can be assessed without the complications of the multimodulus procedures.

Percentage deviations between predicted and measured strains are frequently discussed. Here, percentage deviation is defined as the distance between the measured and predicted strains on the biaxial strain plot divided by the length of a ray from the origin to the measured strain values and is calculated from

$$\%\ \text{Deviation} = \left[\frac{(\epsilon_{a_m} - \epsilon_{a_p})^2 + (\epsilon_{c_m} - \epsilon_{c_p})^2}{\epsilon_{a_m}^2 + \epsilon_{c_m}^2}\right]^{1/2} \times 100\% \quad (2)$$

where a = axial direction, c = circumferential direction, m = measured values, and p = predicted values. The percentage deviation is often preceded by a + or − sign to denote whether the predicted strains are an overestimate (+) or an underestimate (−) of the measured strains. The measured strains, and hence the percentage deviations, are only approximate since most of the experimental results discussed in this section are obtained from graphical results instead of tabulated results.

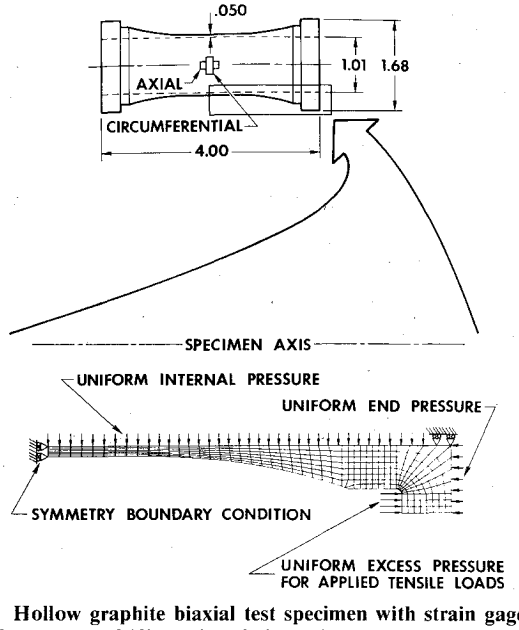

Fig. 6 Hollow graphite biaxial test specimen with strain gages and finite element model (dimensions in inches).

Test Specimen

A typical hollow biaxial test specimen is shown in Fig. 6 (from Fig. 9 of Ref. 8). Internal pressure is applied to the specimen by a pressurizing fluid contained in a thin rubber bladder. Axial loads (either tension or compression) are applied to the specimen at the lips on the specimen ends through a fixture designed to restrict bending. Thus, tests can be performed in two quadrants of biaxial loading. Specimens are loaded to several different ratios of axial stress to circumferential stress (σ_a:σ_c). These nominal stress ratios are approximately constant during loading to a maximum principal thin-wall stress of 3550 psi. The nominal principal material directions are aligned with the load axes for all specimens. The specimen axis (axial load direction) is aligned with the billet axis (z-direction). Strains are measured with strain gages on the outer surface at the midlength of the specimens.

Strain Correlations for Jones-Nelson Nonlinear Material Model Predictions

Strain correlations are performed to determine the applicability of the nonlinear material model to prediction of biaxial stress-strain behavior of ATJ-S graphite. The nonlinear multimodulus material models effectively degenerate to the Jones-Nelson nonlinear material model. This is true either if the material property constants are identical for each independent tension and compression property and the total energy approach is used or if an all-compression or an all-tension stress state exists (with some obvious data input restrictions for the RCM model). In this section, biaxial tension stress states are examined which result from internal pressure and axial tension on the specimen in Fig. 6. Actually, the induced stresses are not all tension, but the radial compressive stress is very small in comparison to the circumferential and axial tensile stresses. Thus, the applicability of the nonlinear material model can be determined without the complications of the multimodulus features of the WCM and RCM models.

The effects of stress gradients in the specimens on the theoretical-experimental comparisons is evaluated by modeling the specimens using the grid with 355 finite elements (provided by Jortner) in Fig. 6. Only half of an actual test

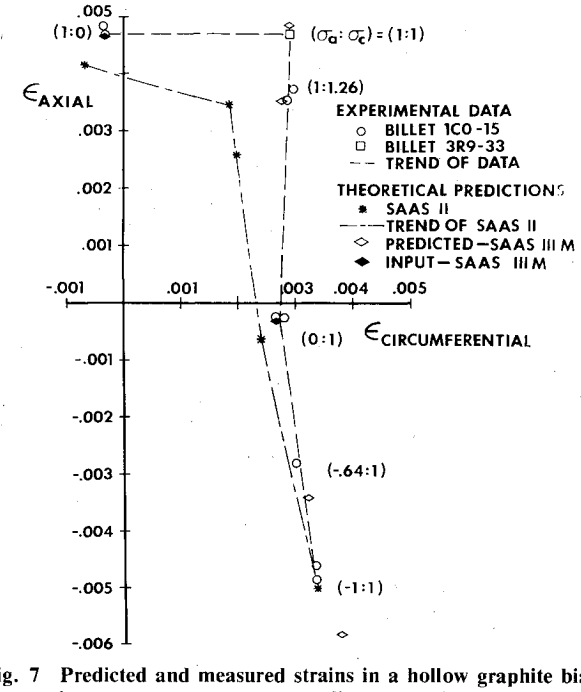

Fig. 7 Predicted and measured strains in a hollow graphite biaxial test specimen—room temperature nonlinear material model.

specimen is modeled because of the symmetry of the specimens and applied loads. This grid is used in a modified version of the SAAS III finite element computer program[13] with the new nonlinear material models. The predicted stresses and strains are fairly uniform in the thin portion of the specimen. However, a slight stress gradient through the specimen wall exists due to bending. Thus, the specimen in Fig. 6 is a good engineering test specimen.

The measured strains and the strains predicted with the nonlinear material model in the SAAS III program are shown in Fig. 7. The measured strain values for a maximum principal thin-wall stress of 3550 psi are Jortner's results[6,9] on the outside of the specimen midlength. The experimental results shown in Fig. 7 are for specimens from a single billet (1C0 − 15) in all but one case. The measured strains for the equal biaxial tension stress state are from a billet 3R9-33 specimen. For the nominal stress ratios (1:1.26) and (−1:1), two data points with slightly different actual stress ratios are shown.

Strain predictions for the nominal stress ratios at a maximum principal thin-wall stress of 3550 psi are shown in Fig. 7 for the nonlinear material model. For the convergence criterion used (relative change in total strain energy ≤ 0.005), the procedure converged in either five or six iterations. Stress and strain gradients can be estimated in the specimens by use of the finite element analysis. The strain predictions shown are extrapolated to the outer surface of the specimens (where the strains were measured) from the center of the element just inside the outer surface.

The SAAS II[14] predictions for a maximum principal thin-wall stress of 3500 psi, as given in Ref. 6, are repeated in Fig. 7 to allow comparison of the new nonlinear material model with the material model now used in reentry vehicle nosetip stress analysis (SAAS II and SAAS III). In the SAAS II material model,[13] a bilinear representation of the uniaxial stress-strain data is used in conjunction with a "normalized effective stress" function to descrive nonlinear orthotropic deformation behavior. There is no explicit assumption of a zero plastic volume change in SAAS II. Instead, the stress function that is used in SAAS II and the unaltered version of SAAS III[13] reduces for isotropic materials to the von Mises distortional energy relation. However, that stress function is an arbitrary expression that cannot be derived, i.e., it has no basis on theoretical grounds. Despite that necessary condition of reduction to a known relation (which is appropriate for isotropic metals but has not been shown to apply to granular materials), the sufficiency condition of applicability to orthotropic materials has *not* been satisfied. Thus, the applicability of the nonlinear material models in the SAAS II and SAAS III computer programs to prediction of stress-strain behavior for ATJ-S graphite is questionable. In addition, the multimodulus character of the material cannot be represented with SAAS II material model. The SAAS III program does have the linear WCM model; however, the nonlinear and multimodulus material models cannot be used simultaneously in SAAS III. Accordingly, any agreement obtained between measured strains and strains predicted with the SAAS II (or SAAS III) material model is both coincidental and fortuitous.

Effects caused by differences in billet stiffness, specimen design, and test procedures in the evaluation of the nonlinear material model are reduced by using, where possible, uniaxial tests of the tubular specimens from billet 1C0-15 to establish the material property constants. The material property constants [A,B,C, and U_0 of Eq. (19) in Ref. 1] for the 5 independent material properties are given in billet coordinates in Table 2. Five independent tension material properties, E_{rt}, E_{zt}, $\nu_{r\theta t}$, $\nu_{z\theta t}$, and G_{rzt}, are used as a data base for the nonlinear material model. Differences between tension and compression material properties are not investigated with the nonlinear procedure. Jortner's across-grain tension results in Fig. 14 of Ref. 9 are used to determine the material property constants for E_{zt} and $\nu_{z\theta t}$. His with-grain tension results in Fig. 17 of Ref. 9 are used to establish the constants for E_{rt} ($=E_{\theta t}$). Values of the two remaining independent material properties are determined from billets other than 1C0-15. Material property constants for $\nu_{r\theta t}$ in Table 2 are identical to those in the 16K9 data base. The remaining material property, G_{rzt}, is $.54\times10^6$ psi and has a negligible effect on the predicted strain results in the test specimen gage sections.

A correction for the circumferential stress gradients is applied to the stress values in Fig. 17 of Ref. 9 before the material property constants for E_{rt} are evaluated. Jortner[9,10] suggests that the circumferential stress at the outer surface of the specimens is approximately related to the mean stress used as the ordinate in Fig. 17 of Ref. 9 by the expression

$$\sigma_{c_{\text{outer surface}}} \cong K\sigma_{c_{\text{mean}}} \tag{3}$$

where $K \cong 0.96 \pm 0.01$. The mean (thin-wall) circumferential stresses are multiplied by 0.96 to obtain an estimate of the circumferential stresses in the specimen at the location where the strains were measured.

The new nonlinear material model is a significant improvement over the previous material model for the two biaxial tension stress ratios investigated. The percentage deviation between test data and predictions for the (1:1) stress ratio is −29.4% for the SAAS II material model and +3.1% for the nonlinear material model. Similar correlation is found for the (1:1.26) stress ratio: a −32% deviation is obtained for the SAAS II nonlinear model and a −2.6% deviation is obtained for the new nonlinear material model. The percentage deviations discussed in this section are based on the measured strains closest to the predicted strains. For both biaxial tension stress ratios, the SAAS II material model predictions are a significant underestimate of the strain response. Obviously, the new nonlinear material model has excellent potential for description of the biaxial softening phenomenon.

Strain predictions with the new nonlinear material model for the (−0.64:1) and (−1:1) stress ratios are poorer than for the biaxial tension stress ratios. However, in those predictions, the multimodulus character of the material is ignored! The deviations between the strain predictions of the new nonlinear material model and the closest experimental results are +15.7% for the (−0.64:1) stress ratio and +18.0% for the (−1:1) stress ratio. Obviously, the different moduli of ATJ-S graphite under tension and compression must be accounted for.

Table 2 1C0 Data base at 70°F for nonlinear material model

Material property	A	B	C	U_0	Data source
E_{rt}	1.85×10^6 psi	0.192	0.314	1 psi	Fig. 17, Ref. 9, 1C0 with circumferential stress gradient adjustment
E_{zt}	1.24×10^6 psi	0.205	0.294	1 psi	Fig. 14, Ref. 9, 1C0
$\nu_{r\theta t}$	0.1	0.376	0.170	1 psi	Fig. 7, Ref. 9, 16K9
$\nu_{z\theta t}$	0.138	0.407	0.0879	1 psi	Fig. 14, Ref. 9, 1C0
G_{rzt}	0.54×10^6 psi	0	1	1 psi	Fig. 28, Ref. 12, Avg.

The apparently good agreement (2.7% deviation) for the SAAS II material model is both coincidental and fortuitous as already discussed. That is, the SAAS II yield criterion is obviously crude and its stress-strain model is only bilinear instead of the actual nonlinear behavior. Those facts, coupled with the poor preditions for the SAAS II model in the biaxial tension quadrant, lead to a complete invalidation of the SAAS II (and the SAAS III) nonlinear material model for ATJ-S behavior.

Strain Correlations for Nonlinear Multimodulus Material Model Predictions with the 16K9 Data Base

The strains measured at room temperature and the strains predicted with the nonlinear weighted compliance material model for a maximum principal thin-wall stress of 3550 psi are shown in Fig. 8. The 16K9 data base in Table 1 is used for predictions because the data for each of the four billets are not complete enough to serve for the nonlinear WCM model. Recall that these data are derived from a portion of the results of Jortner's uniaxial off-axis investigation of billet 16K9. Therefore, the correlation between predicted and measured strains for the stress ratios (1:1.26) and (0:1) is not affected by billet-to-billet variations in material properties.

The experimental data in Fig. 8 are from Fig. 66 of Ref. 6 and Figs. 14-19 of Ref. 9. The measured axial load is in error by less than 1.5% because of friction in the loading apparatus for the biaxial tubular specimens.[9,10] Therefore, the axial stress in the specimen is approximately

$$\sigma_{a_{\text{actual}}} \cong \sigma_{a_{\text{measured}}} \times 1.015 \qquad (4)$$

A similar friction effect is noted for the compression rod results in the data of Table 1. Thus, a friction correction is appropriate for the axial stress components of the (1:0), (1:1), and (1:1.26) stress states. No friction correction need be applied to the axial compression - internal pressure biaxial stresses because the behavior of the biaxial specimens is similar to that of the uniaxial compression rods from which the stress-strain data are obtained. That is, there is no dissimilar behavior as between the uniaxial tension bar and the biaxial specimen under biaxial tension.

The actual experimental strains are obtained for the (1:0) and the (1:1.26) stress ratios in the following manner. The tension stress-strain curve in the axial direction for the biaxial specimen is entered at 50 psi less than the nominal stress, and the corresponding strain is read. A more precise stress correction is unrealistic because the friction error is only approximate and 50 psi is the maximum practical resolution on the plotted stress-strain curves. The circumferential strain for the (1:1.26) biaxial stress is read directly, (i.e., without adjustment for friction). The two strains (axial and circumferential) are then plotted in Fig. 8 with the assumption that they are for the same biaxial load. The experimental strains for the (1:1) stress ratio are plotted without correction because stress-strain curves are not available. Accordingly, results from Fig. 66 of Ref. 6 are used directly. The predicted strains are obtained by use of the nominal stresses.

The predicted strains in Fig. 8 are obtained with the MULTIW computer program.[1] For nominal stress ratios (1:1.26) and (−1:1), two experimental data points with slightly different actual stress ratios are shown. Thus, slightly different strain predictions are obtained for each actual stress ratio. Both strain predictions for the (1:1.26) stress ratio nearly coincide. The predictions shown for the (−1:1) stress ratio are computed for the actual stress ratio of the billet 10V9 results (inverted triangle). Three different sets of strain predictions are shown for each of the two "mixed" stress ratios, (−0.64:1) and (−1:1). The different strain predictions for these stress ratios are a result of the differences in the three energy approaches investigated (total energy, weighted energy with $n=1$, and divided energy). Strain predictions for the (−1:0) stress ratio are shown in Fig. 8 despite the fact that no strains are measured on biaxial specimens at that stress ratio because of possible buckling. These predicted strains for the hollow graphite specimen are based on uniaxial stress-strain data for compression rods. The strain prediction is identical for all energy approaches with the nonlinear WCM model for the (−1:0) stress ratio.

The correlations in Fig. 8 are mainly qualitative in nature because of billet-to-billet variation in material properties. The differences between predicted and measured strain values for the (1:0) stress ratio are attributed mainly to differences in billet stiffnesses. The predicted strains are based on the 16K9 billet data, whereas the measured strains are from tests on specimens from billets 1C0 and 10V9. The strain correlations for the (1:0) stress ratio case lead to the conclusion that billet 16K9 is stiffer in the across-grain (z) direction than either billets 1C0 or 10V9.

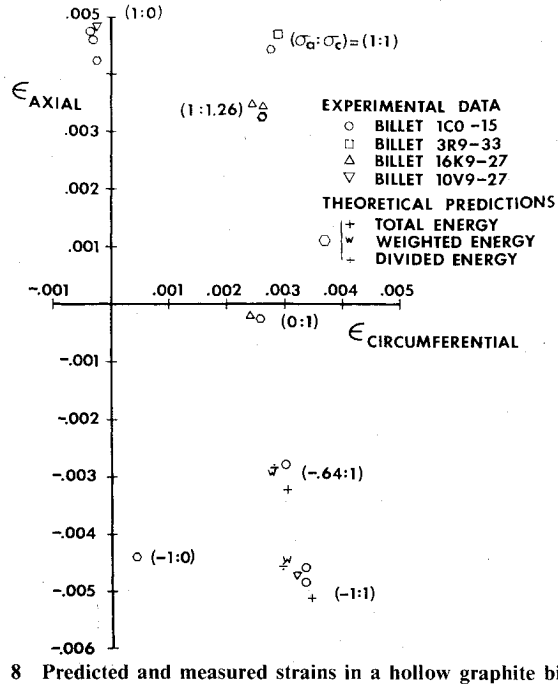

Fig. 8 Predicted and measured strains in a hollow graphite biaxial test specimen—room temperature nonlinear WCM predictions—16K9 data set.

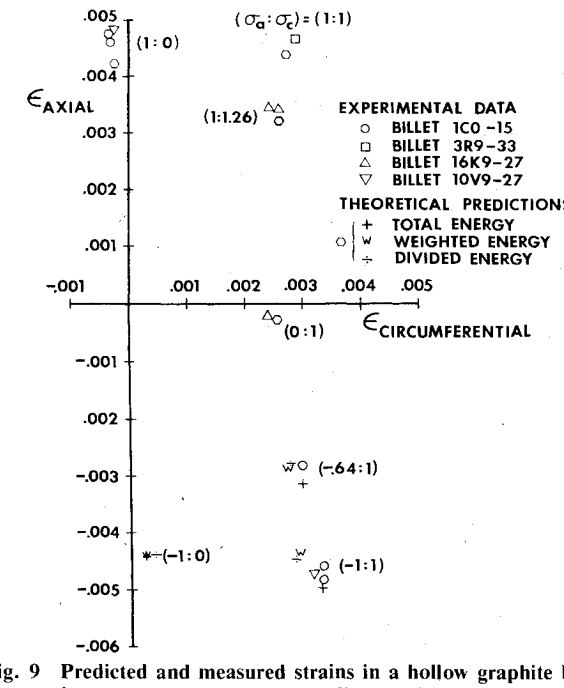

Fig. 9 Predicted and measured strains in a hollow graphite biaxial test specimen—room temperature nonlinear RCM predictions—16K9 data set.

All three energy approaches in the nonlinear WCM model result in identical strain predictions for the (1:0) loading case. Identical strain predictions also result for the other two uniaxial loading cases, (0:1) and (−1:0), and the two biaxial tension loading cases, (1:1) and (1:1.26).

The predicted and measured strains for the equal biaxial tension stress ratio case, (1:1), agree to within 5.5%. Here, again, the strain correlations could be affected by billet-to-billet variations in material properties. For the two (1:1.26) cases, the deviations between predicted and measured strains are 4.6% and 7.4%. Recall that, for these cases and for the (0:1) case, the material properties and the measured strains are obtained from the same billet. Thus, no undesired effects are introduced in the strain correlations by variations in material properties between billets. However, some variations between predicted and measured strain results can be expected due to the gradient in circumferential stress through the thickness of the biaxial test specimens. The stresses at the outer surface of the specimens where the strains are measured can be different from the "thin-wall" stresses used as a basis for the predictions. The circumferential stress gradient could be the major factor in the 7.7% deviation between predicted and measured strains found for the (0:1) stress ratio case. Consistent billets are not used to obtain the predicted and measured strains for the (−0.64:1) and (−1:1) stress ratio case in Fig. 8. Consequently, the predictions for the different energy approaches will not be evaluated until the next section.

Strain predictions for the nonlinear RCM model obtained with the MULTIR computer program[1] and strains measured in room temperature tests are shown in Fig. 9. The strain predictions are for a maximum principal thin-wall stress of 3550 psi. The experimental strains presented in Fig. 9 are identical to those shown in Fig. 8. Material property set E_{zc} described in the off-axis correlations is used for the nonlinear restricted compliance material model. The material property constants for the independent material properties are obtained from billet 16K9 values in Table 1. The predictions with the nonlinear RCM model in Fig. 9 and those with the nonlinear WCM model in Fig. 8 are identical for the biaxial and uniaxial tension cases because of the composition of the E_{zc} property set. When the divided energy approach is used in the nonlinear RCM model with the E_{zc} property set, the transverse strain prediction for the uniaxial compression stress state (−1:0) is different from the common prediction of the total and weighted energy approaches. With the divided energy approach, the implied off-diagonal compliances are always determined from the linear tension material properties.

The strain predictions with the nonlinear WCM and RCM models are different for the mixed biaxial stress states in Figs. 8 and 9. The percentage deviations in the strain predictions with the nonlinear WCM model are used as the baseline values for calculation of percentage deviations. The largest percentage deviation for $(\sigma_a{:}\sigma_c) = (-0.64{:}1)$ and (−1:1) in predicted strains is 3.4% irrespective of the energy approach used. Thus, the effects on strain predictions of the differences in the multimodulus formulations of the two material models are relatively small for the loading conditions and material properties investigated. Accordingly, the agreement between predicted and measured strains found for one material model could be used in a general assessment of both material models.

Strain Correlations for Nonlinear Restricted Compliance Material Model Predictions with the 1C0 Data Base

The experimental strains and two sets of strain predictions (MULTIR and SAAS IIIM) for a maximum principal thin-wall stress of 3550 psi are shown in Fig. 10 for the nonlinear restricted compliance material model. The experimental results shown in Fig. 10 for all but one case are obtained from tests of specimens from billet 1C0-15 in contrast to Figs. 8 and 9. The strains measured for the equal biaxial tension stress state are from billet 3R9-33.

Effects of differences in billet stiffness, specimen design, and test procedures in the evaluation of the nonlinear multimodulus material models are reduced by using, where possible, uniaxial tests of the turbular specimens to establish the material property constants. The material property constants [A, B, C, and U_o of Eq. (19) of Ref. 1,] for the six independent material properties in the nonlinear RCM model property set E_{zc} are given in billet coordinates in Table 2 supplemented by the values for E^{45}_{rzl} ($A = 1.39\times10^6$ psi, $B = 0.133$, $C = 0.365$, and $U_o = 1$ psi) from Fig. 5 of Ref. 9 for billet 16K9 and for E_{zc} ($A = 1.04\times10^6$ psi, $B = 0.114$, $C = 0.444$, and $U_o = 1$ psi) from Fig. 9 of Ref. 9 for billet 16K9 (adjusted for billet 1C0 stiffness) in place of the values for G_{rzl} in Table 2. These material property constants are used to obtain both sets of predictions for the nonlinear RCM model. As is the case with $\nu_{r\theta l}$, material property constants for E^{45}_{rzl} are obtained from results from billet 16K9 instead of 1C0. Consequently, the material property constants for $\nu_{r\theta l}$ and E^{45}_{rzl} are identical in both the 16K9 (Table 1), and 1C0 (Table 2 plus supplement) data bases.

Material property constants for E_{zc} are obtained from billet 16K9. Uniaxial stress-strain results are not available for the tube specimens from billet 1CO under compression loading (the specimens would buckle!) Thus, an adjustment for the apparent difference in stiffnesses of billets 16K9 and 1CO is made. The uniaxial strain results in Fig. 9 of Ref. 9 are obtained from across-grain compression loading of the rod specimens from billet 16K9. At a given stress, the strain from Fig. 9 of Ref. 9 is multiplied by the ratio of the strains found in across-grain uniaxial tension tests of tube specimens from billet 1C0, and rod specimens from billet 16K9. The resulting strain is used to evaluate the material property constants for E_{zc}.

The 1C0 data base is used with both nonlinear RCM model prediction techniques considered in Fig. 10. The procedures converge in four to six iterations for each of the cases analyzed for the convergence criterion used in the MULTIR and modified SAAS III programs (relative change in total strain energy ≤ 0.005). Recall that the differences in predictions with the two nonlinear RCM model approaches are due to stress gradients in the specimens. The circumferential

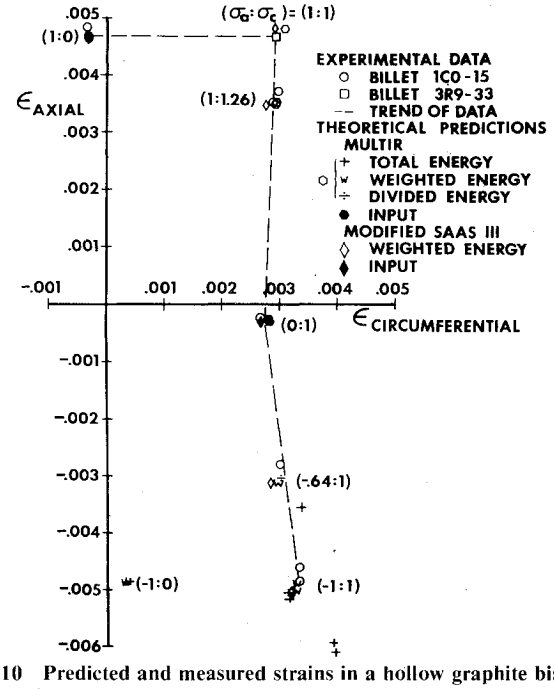

Fig. 10 Predicted and measured strains in a hollow graphite biaxial test specimen—room temperature nonlinear RCM predictions—1C0 data set.

strains predicted with the 355 element grid in the SAAS III program are between 4% and 6% less than those predicted with the MULTIR program with the same energy approach.

Strains predicted with the nonlinear RCM model agree well with measured strains for the two biaxial tension stress ratios investigated with the modified SAAS III approach. For the equal biaxial tension stresses, predicted and measured strains differ by 3%. The predictions with the modified SAAS III approach for the nominal (1:1.26) stress ratio are based on the stress ratio of the upper of the two data points. Those predictions are 7% less than the experimental strains. If, instead, the stress ratio of the lower experimental point were used, better (but not significantly better) correlation would be obtained. This speculation is based on the observation that the two predictions with the MULTIR program are essentially on top of one another; a similar result is expected for the modified SAAS III results.

The actual ratio of axial stress to circumferential stress for the two data points with a nominal (1:1.26) stress ratio in Fig. 10 is slightly smaller for the upper point than for the lower point. When the circumferential stress is 3550 psi in Fig. 16 of Ref. 9, then the axial stress in Fig. 15 of Ref. 9 for the upper experimental data point in Fig. 10 is lower than the axial stress for the lower point. The upper point has the largest strains, but corresponds to a lower axial stress in contradiction to the expected stress-strain behavior. Thus, the differences between the two experimental points for the nominal (1:1.26) stress ratio are probably data scatter and not a result of differences in actual stress levels. Given the scatter expected in experimental results, a 7% deviation may represent good agreement.

For the (1:1.26) stress ratio, the strain predictions with the nonlinear material model shown in Fig. 7 are not identical to the strain predictions with the nonlinear RCM model shown in Fig. 10 mainly because different stress ratios are used. However, even for identical stress ratios, a small difference could occur between the two sets of predictions. A radial stress gradient exists through the thickness of the specimen. Thus, a triaxial stress state must actually be analyzed. Different material properties are used to determine the compliances in the two material models since the radial stress is a compressive principal stress.

In the biaxial loading quadrant with mixed tension and compression loading, the correlation between predicted and measured strain response is dependent on the energy approach used. The percentage deviations from the experimental strain results for the (−0.64:1) data point and one of the (−1:1) data points are presented in Table 3. Results for both the MULTIR and the modified SAAS III formulations of the nonlinear RCM model are shown. Percentage deviations are given for the MULTIR program with all three of the energy approaches. Only the weighted energy approach is used with the modified SAAS III program. The actual stress ratios for the two (−1:1) data points are (−0.97:1) and (−0.99:1). The effects of stress gradients in the specimens on the predicted strain response are determined for the (−0.99:1) stress ratio with the nonlinear RCM model in the modified SAAS III computer program. The lower of the two (−1:1) experimental points shown in Fig. 10 is the strain result for the (−0.99:1) stress ratio. Thus, the strain predictions denoted by the diamond symbol must be compared with the experimental strains for the lower of the two circles.

Table 3 Percentage deviations of nonlinear RCM model strain predictions from measured strains

	Percentage deviations			
	MULTIR			Modified SAAS III
Loading (σ_a:σ_c)	Total energy	Weighted energy	Divided energy	Weighted energy
(−.64:1)	20.2	8.3	6.1	9.0
(−.99:1)	23.5	3.2	6.5	4.3

The weighted or divided energy approaches with deviations of 3-9% in Table 3 are superior to the total energy approach with deviations of 20-24%. A recommendation as to which approach should be generally used, the divided energy or the weighted energy, cannot be made based solely on the percentage deviations in Table 3. However, from the standpoint of the theoretical formulations and limitations of the nonlinear RCM model, the weighted energy approach might be preferable. With the weighted energy approach, all material properties are evaluated at the same energy level. In that manner, the additional restrictive implications of the evaluation of tension and compression material properties at different energy levels are avoided.

Summary

Biaxial strain predictions with the various nonlinear material models described in this paper are compared with several types of experimental data. The comparisons with room temperature data are for biaxial tension and mixed tension and compression at a maximum principal thin-wall stress of 3550 psi. The room temperature biaxial tension predictions are within about 3% of the experimental results. Thus, the basic relationship between the secant moduli of the nonlinear stress-strain curves and the strain energy is shown to be accurate. Accordingly, the phenomenon of softening under biaxial tension is now predictable with the new material model.

Extensions of the new material model to different room temperature behavior in tension and compression are not quite as accurate as in biaxial tension. The strain predictions are fairly good (within 9%), however, when the weighted energy or divided energy approaches are used in the nonlinear RCM model as opposed to the total energy approach. The predictions with the nonlinear WCM model are slightly different from those with the nonlinear RCM model for the loading and material properties considered. However, uniaxial stress-strain data are often not sufficient to apply the nonlinear WCM model.

Concluding Remarks

Two new nonlinear multimodulus material models developed by Jones and Nelson[1] are correlated with experimental strain results for ATJ-S graphite to determine the accuracy of the models. The experimental results are due to Jortner[6-10] and consist of strains from uniaxial loading of bar and rod specimens in nonprincipal material directions and from biaxial loading of tubular specimens. The predicted strains for uniaxial off-axis loading and biaxial loading agree very well with measured strains. In fact, the agreement is surprisingly good for such a highly nonlinear deformation problem that is also complicated by different behavior in tension than in compression.

The application and evaluation of the new material models is hampered by the lack of suitable uniaxial stress-strain data to determine material property constants in the general nonlinear stress-strain relations. Poisson's ratio data are inadequate to properly establish the variation with strain energy. All complexities of data acquisition are multiplied by two when multimodulus materials are considered. That is, all data must be gathered under tension as well as under compression loading. Moreover, a new parameter, the Young's modulus at 45° to principal material directions, must be measured in both tension and compression. These new moduli are the replacement for the usual shear modulus.

Two nonlinear multimodulus material models are used in prediction of uniaxial deformation behavior of ATJ-S graphite for loads applied at various angles from principal material directions (off-axis tests). When these predictions are compared with the strain response measured by Jortner,[9] the best overall correlation exists for the nonlinear weighted com-

pliance matrix model. Differences between measured strains and the predictions with the nonlinear restricted compliance matrix model are attributed mainly to the restrictions on tension and compression compliances inherent to the model. That is, the stress-strain behavior of ATJ-S graphite does not closely fit the restrictions on tension and compression compliances. Different strain predictions are obtained when mainly tension compliances are used and compression compliances are generated by use of the restrictions than when mainly compression compliances are used. At 5000 psi, differences of 8 to 12% in axial strain predictions occur between the two types of predictions. Accordingly, the nonlinear weighted compliance matrix model is preferable to the nonlinear restricted compliance matrix model for graphite.

The strain correlations for the nonlinear restricted compliance matrix model with either the weighted energy or divided energy approach are within 9% for biaxial loading cases with mixed tensile and compressive principal stresses at room temperature. Strains are overpredicted by about 20% with the total strain energy approach. The predictions with the two nonlinear multimodulus material models (with the same energy approach) are only slightly, if at all, different for the biaxial stress states investigated. Thus, similiar strain correlations are anticipated for the nonlinear weighted compliance model.

The experimental biaxial results are few in number and exist in only two quadrants of biaxial loading. Thus, comprehensive validation of the nonlinear multimodulus material models must wait future experimental investigation. Study of ATJ-S graphite behavior in the biaxial loading quadrants with 1) axial and circumferential compression and 2) axial tension and circumferential compression is recommended. Without such a study, the possible hardening of graphite under biaxial compression (as opposed to softening under biaxial tension) cannot be confidently predicted.

The nonlinear weighted compliance matrix model with the weighted energy approach is recommended for use in graphite stress analysis. This recommendation is based on the fact that better strain correlation exists for that model than for the nonlinear restricted compliance matrix model. The lack of success with the latter model is probably due to the fact that the compliance restrictions are not satisfied for graphite material properties. The nonlinear weighted compliance matrix model should be regarded as an engineering approach to the nonlinear deformation problem. The various energy approaches (weighted energy, etc.) fall in the same category as opposed to the more scientific, but unsubstantiated, approach of the restricted compliance matrix model.

References

[1] Jones, R.M. and Nelson, D.A.R., Jr., "Material Models for Nonlinear Deformation of Graphite," *AIAA Journal,* Vol. 14, June 1976, pp. 709-717.

[2] Jones, R.M., "Stress-Strain Relations for Materials with Different Moduli in Tension and Compression," *AIAA Journal,* Vol. 14, Dec. 1976, to be published.

[3] Isabekian, N.G. and Khachatryan, A.A., "On the Multimodulus Theory of Elasticity of Anisotropic Bodies in a Plane Stress State," *Isvestiya akademii nauk armianskoi SSR, Mekhanika,* No. 5, 1969, pp. 25-34. IAA Accession Number A70-22152. Translation available from Robert M. Jones, SMU Institute of Technology, Dallas, Texas.

[4] Jones, R.M. and Nelson, D.A.R., Jr., "A New Material Model for the Nonlinear Biaxial Behavior of ATJ-S Graphite," *Journal of Composite Materials,* Jan. 1975, pp.10-27.

[5] Jones, R.M. and Nelson, D.A.R., Jr., "Further Characteristics of a Nonlinear Material Model for ATJ-S Graphite," *Journal of Composite Materials,* July 1975, pp. 251-265.

[6] Jortner, J.R., *Multiaxial Behavior of ATJ-S Graphite,* McDonnell-Douglas Astronautics Co., Air Force Materials Lab. Rep. AFML-TR-71-253, Dec. 1971, Wright-Patterson AFB, Ohio.

[7] Jortner, J., *Biaxial Mechanical Properties of ATJ-S Graphite,* Final Report under AF Contract F04701-068-C-0288, Change Order 15, McDonnell-Douglas Rept. MDC G2072, Dec. 1970, Santa Monica, Calif.

[8] Jortner, J., *Multiaxial Behavior of ATJ-S Graphite,* McDonnell-Douglas Astronautics Co., Air Force Material Lab. Rept. AFML-TR-71-160, July 1971, Wright-Patterson AFB, Ohio.

[9] Jortner, J., *Uniaxial and Biaxial Stress-Strain Data for ATJ-S Graphite at Room Temperature,* McDonnell-Douglas Astronautics Co., Rept. MDC G3564, June 1972, Huntington Beach, Calif.

[10] Jortner, J., *Multiaxial Response of ATJ-S Graphite,* McDonnell-Douglas Astronautics Company, Air Force Materials Lab. Rept. AFML-TR-73-170, Oct. 1973, Wright-Patterson AFB, Ohio.

[11] Jones, R.M. and Nelson, D.A.R. Jr., *Nonlinear Deformation of Graphitic Materials,* SMU Institute of Technology, Dallas, Texas, Air Force Materials Lab. Rept. AFML-TR-74-259, Feb. 1975, Wright-Patterson AFB, Ohio.

[12] Starrett, H.S. and Pears, C.D., *Probable and Average Properties of ATJ-S (WS) Graphite,* Southern Research Institute, AFML-TR-73-14, Vol. 1, Feb. 1973, Wright-Patterson AFB, Ohio.

[13] Crose, J.G. and Jones, R.M. *SAAS III, Finite Element Stress Analysis of Axisymmetric and Plane Solids with Different Orthotropic, Temperature-Dependent Material Properties in Tension and Compression,* TR-0059 (S6816-53)-1, The Aerospace Corp., San Bernardino, Calif., June 1971.

[14] Jones, R.M. and Crose, J.G. *SAAS II, Finite Element Stress Analysis of Axisymmetric Solids with Orthotropic, Temperature-Dependent Material Properties,* TR-0200(S4980)-1, The Aerospace Corp., San Bernardino, Calif. Sept. 1968.